Semiconductor Science and Technology

PAPER

Valence and conduction band offsets for sputtered AZO and ITO on (010) $(Al_{0.14}Ga_{0.86})_2O_3$

To cite this article: Chaker Fares *et al* 2019 *Semicond. Sci. Technol.* **34** 025006

IOP Publishing Semiconductor Science and Technology
Semicond. Sci. Technol. 34 (2019) 025006 (8pp) https://doi.org/10.1088/1361-6641/aaf8d7

Valence and conduction band offsets for sputtered AZO and ITO on (010) $(Al_{0.14}Ga_{0.86})_2O_3$

Chaker Fares[1], F Ren[1], Eric Lambers[2], David C Hays[2], B P Gila[2,3] and S J Pearton[3,4]

[1] Department of Chemical Engineering, University of Florida, Gainesville, FL 32611 United States of America
[2] Nanoscale Research Facility, University of Florida, Gainesville, FL 32611 United States of America
[3] Department of Materials Science and Engineering, University of Florida, Gainesville, FL 32611 United States of America

E-mail: spear@mse.ufl.edu

Received 24 September 2018, revised 7 December 2018
Accepted for publication 17 December 2018
Published 10 January 2019

Abstract

$(Al_xGa_{1-x})_2O_3/Ga_2O_3$ metal-oxide semiconductor field effect transistors are emerging as candidates for rf and power electronics, but a drawback is the high contact resistances on these wide bandgap semiconductors. A potential solution is to use narrower gap transparent conducting oxides such as IZO and ATO to reduce the interfacial resistance. In this paper, we report the measurement of the valence band offset of the AZO/$(Al_{0.14}Ga_{0.86})_2O_3$ and ITO/$(Al_{0.14}Ga_{0.86})_2O_3$ heterointerfaces using x-ray Photoelectron Spectroscopy. The single-crystal β-$(Al_{0.14}Ga_{0.86})_2O_3$ was grown by molecular beam epitaxy. The bandgaps of the sputter-deposited AZO and ITO were determined by reflection electron energy loss spectroscopy to be 3.2 ± 0.20 and 3.5 ± 0.20 eV, respectively, while high resolution XPS data of the O 1s peak and onset of elastic losses was used to establish the $(Al_{0.14}Ga_{0.86})_2O_3$ bandgap as 5.0 ± 0.30 eV. The valence band offsets were −0.59 eV ± 0.10 eV and −1.18 ± 0.20 eV, respectively, for AZO and ITO. The conduction band offsets were 1.21 ± 0.25 eV for AZO, and 0.32 ± 0.05 eV for ITO. Both were of the straddling gap, type I alignment on β-$(Al_{0.14}Ga_{0.86})_2O_3$ and all the offsets are negative, consistent with achieving improved electron transport across the heterointerface.

Keywords: gallium oxide, band offset, aluminum gallium oxide

(Some figures may appear in colour only in the online journal)

Introduction

β-Ga_2O_3 is under development for power switching and control electronics as well as solar blind UV detection [1–11]. The β polymorph of Ga_2O_3 has a bandgap of ~4.8 eV and is commercially available in large diameter bulk and epitaxial form [1–3, 8]. The absence of p-type doping capability [12, 13] has led to a focus on vertical Schottky rectifiers and gate all-around FinFET-like devices which operate in accumulation mode in the on-state [1, 3–5, 7–10]. Additionally for lateral devices, the $(Al_xGa_{1-x})_2O_3/Ga_2O_3$ heterostructure has been recently demonstrated using modulation doping of the barrier layer [14–21], as β-Ga_2O_3 is nonpolar. There is strong interest in these heterostructures involving β-$(Al, Ga)_2O_3$ monoclinic phase alloys, in which the bandgap can be varied from 4.8 to 6 eV [14–21]. Typically, the x value is between 0.12 and 0.18 in the alloys. One of the drawbacks of β-$(Al_xGa_{1-x})_2O_3/Ga_2O_3$ heterostructures is the high contact resistances encountered when fabricating Ohmic contacts [14–20].

One potential method for reducing the contact resistance is to include a lower gap transparent conducting oxide as an interlayer between the metal and the wide bandgap semiconductor [22–27]. The most commonly used TCOs are indium tin oxide (ITO) and aluminum zinc oxide (AZO).

[4] Author to whom any correspondence should be addressed.

Sputtered films of both of these materials have been reported as intermediary layers for forming Ohmic contacts on Ga_2O_3 [22, 25, 27]. The use of Pt/ITO bi-layers to β-Ga_2O_3 improved the Ohmic contact properties compared to Pt/Ti through formation of an interfacial layer with lower bandgap and higher doping concentration than the Ga_2O_3 [22]. AZO interlayers are also proven effective in lowering contact resistance of Ti/Au contacts on n-type, Si implanted β-Ga_2O_3. A specific contact resistance of $2.82 \times 10^{-5}\,\Omega\,cm^2$ was reported for annealing at 400 °C, while Ti/Au contacts without the AZO interlayer did not lead to Ohmic behavior [25]. The band alignment at the heterointerfaces is obviously critically important in determining the favorability of carrier transport [28–39]. Currently, there have been no reports for the band alignments of these TCOs on $(Al_xGa_{01-x})_2O_3$.

In this paper, we report on the determination of the band alignment in the AZO/$(Al_{0.14}Ga_{0.86})_2O_3$ and ITO/$(Al_{0.14}Ga_{0.86})_2O_3$ heterostructures, in which the TCOs were deposited by sputtering onto $(Al_{0.14}Ga_{0.86})_2O_3$ grown by molecular beam epitaxy (MBE). This alloy composition is typical of that used in heterostructure transistors. The valence band offset was obtained from XPS measurements [40] and by measuring the respective bandgaps of the TCOs, we obtained the conduction band offset in the heterostructures and determined the band alignment type.

Experimental

1.5 nm AZO or ITO was deposited by RF magnetron sputtering on the $(Al_{0.14}Ga_{0.86})_2O_3/Ga_2O_3$ structures and thicker layers (150 nm) on quartz substrates at room temperature using 3 in. diameter composite ITO (In_2O_3/SnO_2 90/10) or AZO (Al_2O_3/ZnO_2 2/98 wt%) targets. The RF power was 125 W and the working pressure was 5×10^{-6} Torr in a pure Ar ambient. The DC bias on the electrode under these conditions is in the range of 30–40 V. Both thick (150 nm) and thin (1.5 nm) layers of the dielectrics were deposited to be able to measure both bandgaps and core levels on the β-$(Al_{0.14}Ga_{0.86})_2O_3$. Hall measurements on the thick AZO films showed resisitivity of $7.4\,\Omega\,cm^{-1}$, carrier concentration of $1.78 \times 10^{18}\,cm^{-3}$ and Hall mobility of $26\,cm^2\,V^{-1}\,s^{-1}$. X-ray diffraction 2θ scans showed a (002) peak at 34.3°, indicative of a [001] preferred orientation with the *c*-axis perpendicular to the substrate, similar to previous reports [41]. The thick ITO, XRD showed peaks due to (400) and (222), indicating the coexistence of [100] and [111] textures [42, 43]. The resistivity was $2.6 \times 10^{-1}\,\Omega\,cm$, with Hall mobility of $19\,cm^2\,V^{-1}\,s^{-1}$ and carrier concentration of $9 \times 10^{16}\,cm^{-3}$. For substrate cleaning pre-deposition, the following rinse sequence was employed: acetone, IPA, N_2 dry, and finally Ozone exposure for 15 min. These films were deposited onto epi $(Al_{0.14}Ga_{0.86})_2O_3$ that was grown by MBE. The sample was grown by oxygen plasma-assisted MBE using a Ga flux of 6×10^{-8} Torr, Al flux of 2×10^{-8} Torr, an oxygen plasma power of 280 W and a chamber pressure of 1.2×10^{-5} Torr. Under these conditions it is possible to maintain the phase purity of the alloy [44]. These AGO $(Al_{0.14}Ga_{0.86})_2O_3$ layers were doped with Si to produce an n-type carrier density of $10^{17}\,cm^{-3}$, with mobility of $180\,cm^2\,V^{-1}\,s^{-1}$ at room temperature and were 55 nm thick. The donor concentration was determined by electrochemical capacitance–voltage profiling at a frequency of 740 Hz on calibration samples and the composition was determined by x-ray diffraction on these same samples [44]. These epitaxial layers were grown on top of Sn-doped ($6.3 \times 10^{18}\,cm^{-3}$) bulk β-phase Ga_2O_3 single crystal substrates (500 μm thick) with (010) surface orientation grown by the edge-defined film-fed growth method. The heterostructure samples are shown schematically in figure 1.

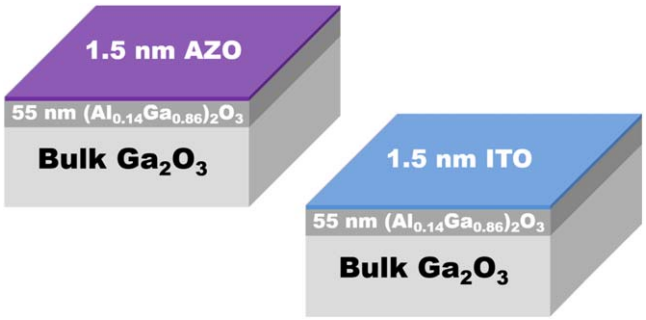

Figure 1. Layer structure of the heterostructures used in this work.

The chemical state of the ITO, AZO, and β-$(Al_{0.14}Ga_{0.86})_2O_3$ and identification of peaks for high resolution analysis were obtained from XPS survey scans in a ULVAC PHI XPS system. This employs a monochromatic, Al x-ray source (energy 1486.6 eV) at a source power of 300 W. The analysis area was 10 μm in diameter with a take-off angle of 50° and an acceptance angle of ±7°. The electron pass energy was 23.5 eV for the high-resolution scans and 93.5 eV for the survey scans.

Charge compensation was achieved with a dual beam charge neutralization system with simultaneous low-energy electron and ion beams [45]. Using the position of the adventitious carbon (C–C) line in the C 1s spectra at 284.8 eV, charge correction was performed. During the measurements, the samples and electron analyzers were electrically grounded to provide a common reference Fermi level. Differential charging is a concern for semiconductor band offset measurements [45] and while use of an electron flood gun does not guarantee that differential charging is not present, our experience with oxides on conducting substrates has been that the differential charging is minimized with the use of an electron gun. Calibrations without the guns verified that was the case [36].

Reflection electron energy loss spectroscopy (REELS) was employed to measure the bandgap of the AZO and ITO [46]. By taking a linear fit to the leading plasmon peak and finding its zero energy with the background, a direct measurement of valence to conduction band energy is made. REELS spectra were obtained using a 1 kV electron beam and the hemispherical electron analyzer.

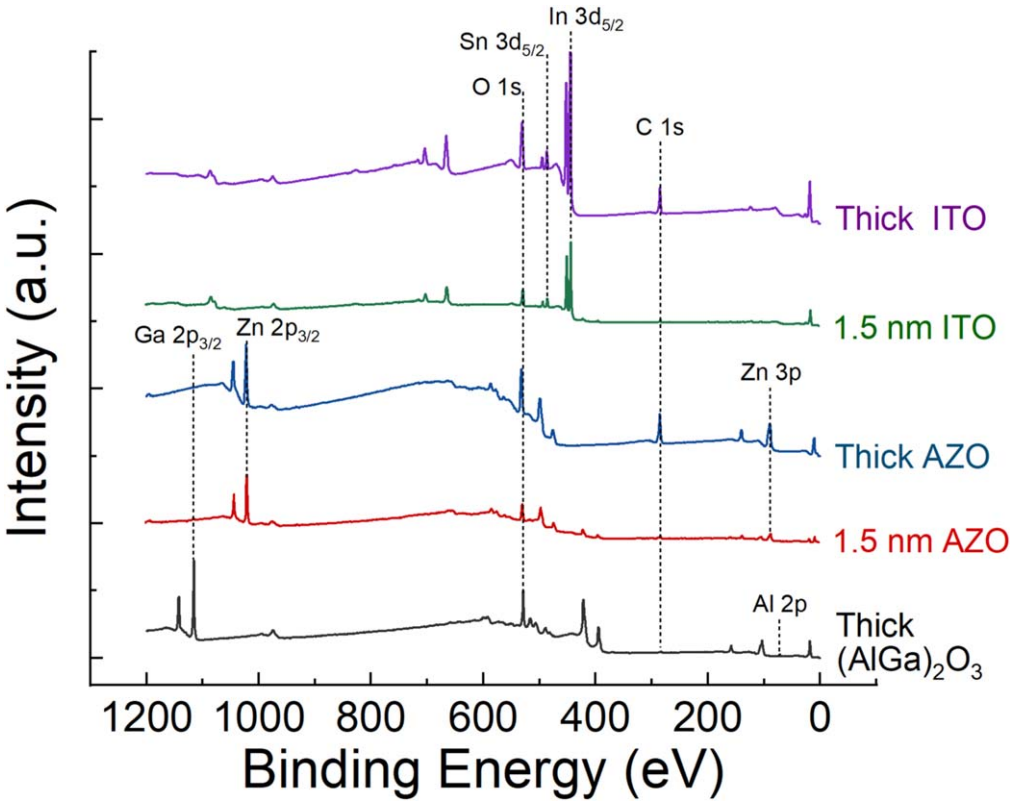

Figure 2. XPS survey scans of thick sputtered AZO and ITO, 1.5 nm sputtered AZO and ITO on $(Al_{0.14}Ga_{0.86})_2O_3$, and a $(Al_{0.14}Ga_{0.86})_2O_3$ reference sample. The intensity is in arbitrary units (a.u.).

Results and discussion

Figure 2 shows the stacked XPS survey scans of thick (150 nm) AZO and ITO, 1.5 nm AZO and ITO on β-$(Al_{0.14}Ga_{0.86})_2O_3$, and an $(Al_{0.14}Ga_{0.86})_2O_3$ reference sample. There is no evidence of metallic contamination from the sputtering process, which if present in sufficient quantities can form oxides that reduce the overall bandgap of the dielectrics and affect the resulting band alignment [47–50].

We obtained the valence band maximum (VBM) from linear fitting of the leading edge of the valence band and the flat energy distribution from the XPS measurements, and finding the intersection of these two lines [40, 49]. This is shown in figure 3 for the thick AZO and ITO, and the $(Al_{0.14}Ga_{0.86})_2O_3$. The VBMs were measured to be 3.0 ± 0.2 eV for β-$(Al_{0.14}Ga_{0.86})_2O_3$, 2.53 ± 0.4 eV for the AZO and 2.74 eV $\pm$ 0.4 eV for the ITO.

The measured bandgaps for the AZO and ITO were 3.2 ± 0.30 eV and 3.5 ± 0.30 eV, respectively, from the REELS data of figure 4. The bandgap of the β-$(Al_{0.14}Ga_{0.86})_2O_3$ was determined to be 5.0 ± 0.3 eV, from XPS O1s based electron energy loss measurements [40, 41]. This is consistent with past work on powdered samples of $(Al_xGa_{1-x})_2O_3$ over the composition range $x = 0$–0.4 [51]. If we use the theoretical relationship derived by Peelaers *et al* [29], we would expect a bandgap of 5.14 eV at our composition of $x = 0.14$, close to the measured result. The difference in bandgaps between AZO and ITO and β-$(Al_{0.14}Ga_{0.86})_2O_3$ are therefore 1.8 and 1.5 eV, respectively, and then it is necessary to determine how these are partitioned between valence and conduction bands.

To determine the band alignment, we used the standard core level spectra approach due to Kraut *et al* [40]. This method relies on precise measurement of a core level and the valence band edge for each material investigated and the shift of the core levels when the two materials have formed the heterojunction. The equation used to calculate the offset is:

$$\Delta E_V = (E^1_{\text{core}} - E^1_{\text{VBM}}) - (E^2_{\text{core}} - E^2_{\text{VBM}}) - (E^1_{\text{core}} - E^2_{\text{core}}).$$

It is important to use a well-defined core level since the offsets are small compared to the core level energy and more deviation is expected at higher core level energies.

High resolution XPS spectra of the VBM-core delta region are shown in figure 5 for the β-$(Al_{0.14}Ga_{0.86})_2O_3$ and thick AZO and ITO samples. These were used to determine the selected core level peak positions. Figure 6 shows the XPS spectra for the β-$(Al_{0.14}Ga_{0.86})_2O_3$ to AZO and ITO core delta regions of the heterostructure samples. These values are summarized in table 1 and were then used to calculate ΔE_v.

Figure 7 shows the band alignment of the AZO/β-$(Al_{0.14}Ga_{0.86})_2O_3$ and ITO/β-$(Al_{0.14}Ga_{0.86})_2O_3$ heterostructures. Both are nested, type I systems. The valence band offset is -0.59 ± 0.10 eV and conduction band offset is -1.21 ± 0.25 eV for the AZO/β-$(Al_{0.14}Ga_{0.86})_2O_3$. For the ITO/$\beta$-$(Al_{0.14}Ga_{0.86})_2O_3$ heterostructure, the values are -1.18 ± 0.20 eV for valence band offset and -0.32 ± 0.05 eV for the conduction band offset. These were obtained using the

Table 1. Summary of measured core levels in these experiments (eV).

Reference $(Al_{0.14}Ga_{0.86})_2O_3$				Reference dielectric				Thin dielectric on $(AlGa)_2O_3$	
Core level	VBM	Core level peak	Core-VBM	Film (Core)	VBM	Core level peak	Core-VBM	Δ Core level	Valence band offset
$Ga2p_{3/2}$	3.00	1117.60	1114.60	AZO (Zn 2p3)	2.53	1021.92	1019.39	95.8	−0.59
				ITO (In 3d5)	2.74	445.12	442.38	673.4	−1.18

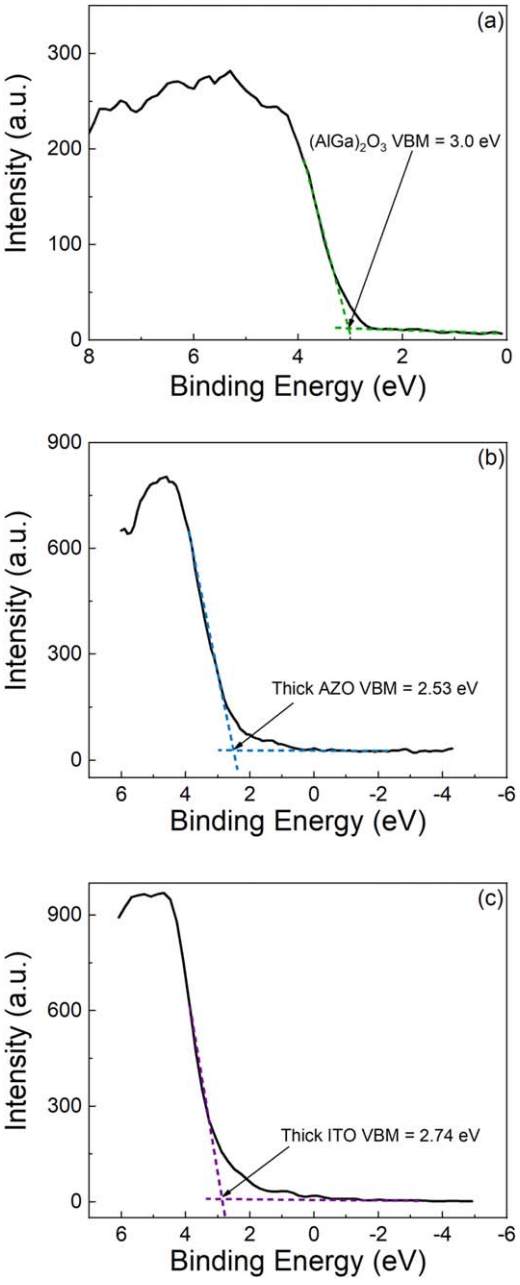

Figure 3. XPS spectra of core levels to valence band maximum (VBM) for (a) reference $(Al_{0.14}Ga_{0.86})_2O_3$, (b) thick film sputtered AZO, and (c) thick film sputtered ITO. The intensity is in arbitrary units (a.u.).

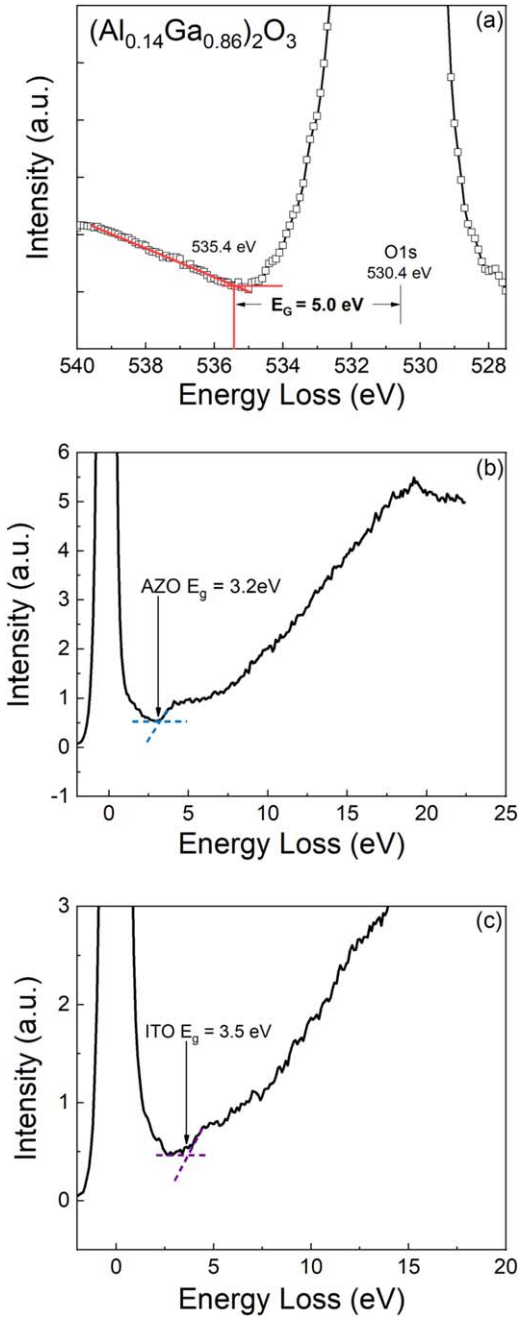

Figure 4. Bandgap of (a) $(Al_{0.14}Ga_{0.86})_2O_3$ determined by the onset of energy loss spectrum. Bandgap of sputtered (b) AZO and (c) ITO determined by RHEELS data. The intensities are in arbitrary units (a.u.).

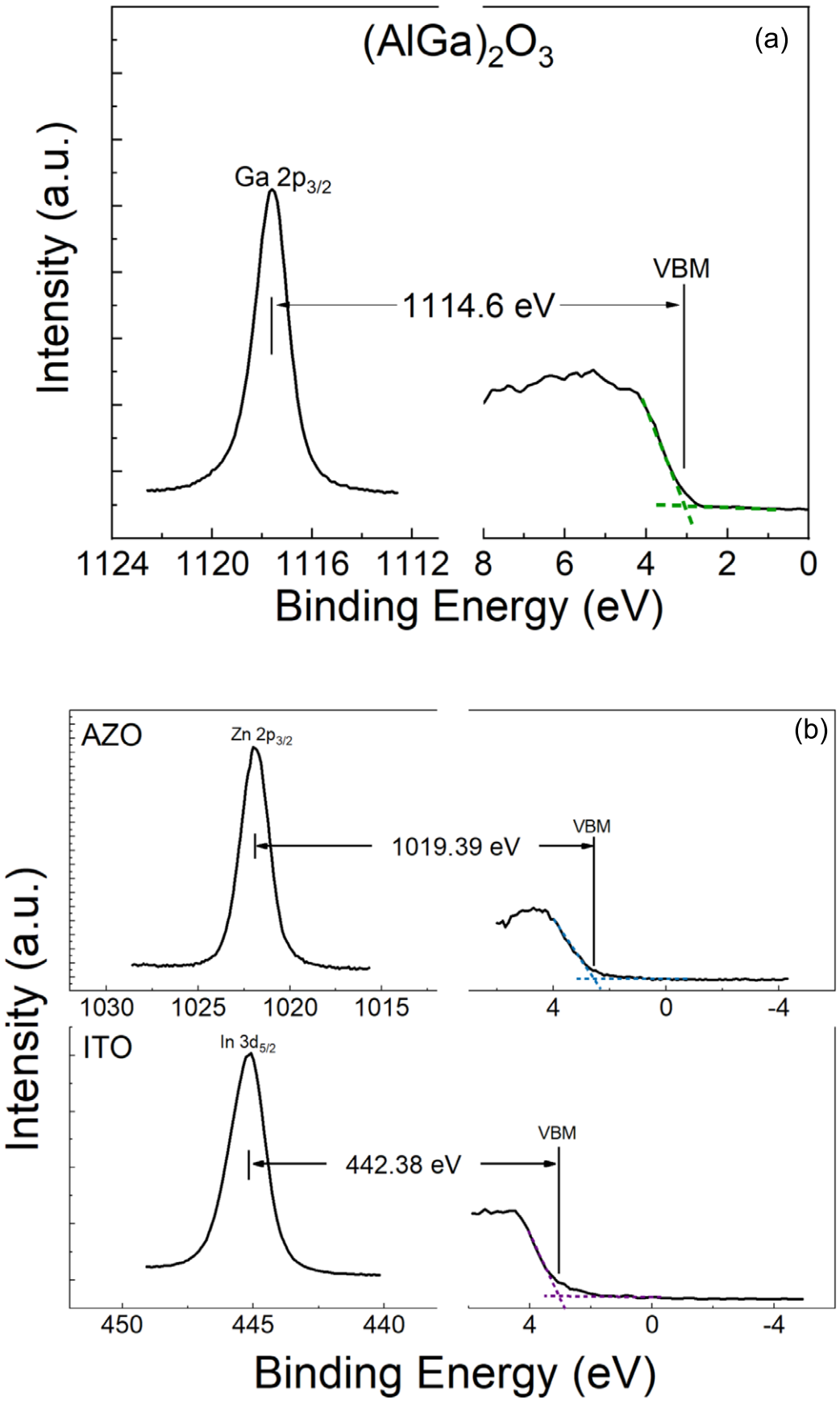

Figure 5. High resolution XPS spectra for the vacuum-core delta regions of (a) $(Al_{0.14}Ga_{0.86})_2O_3$ and (b) sputtered AZO and ITO films. The intensity is in arbitrary units (a.u.).

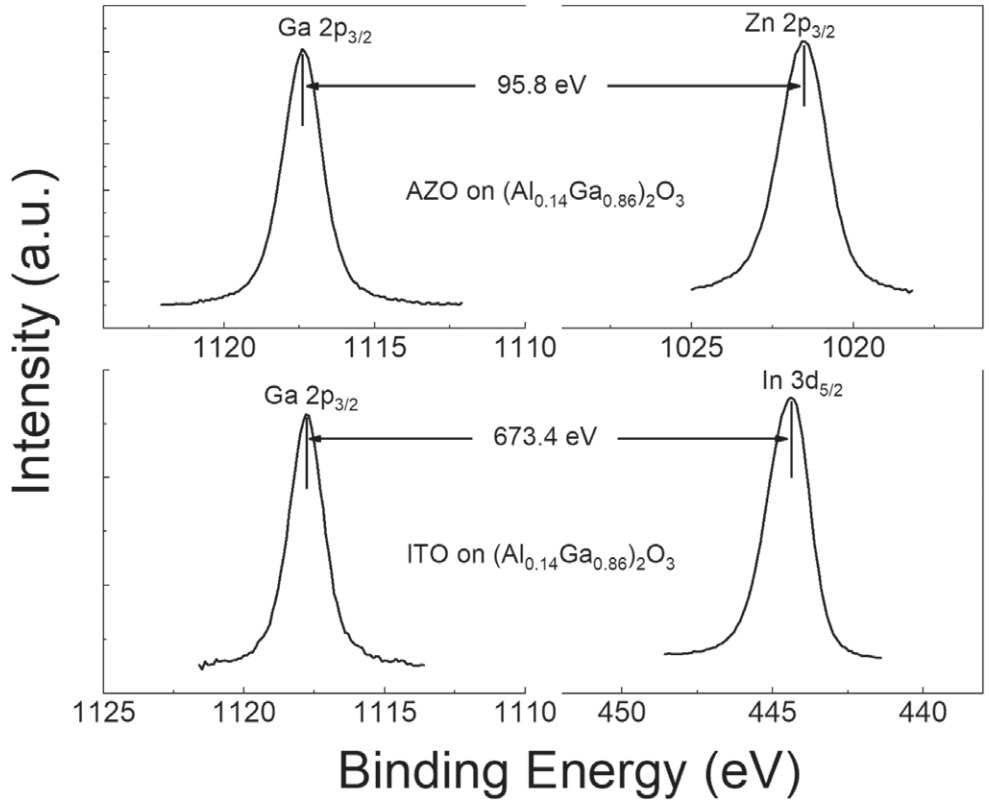

Figure 6. High resolution XPS spectra for the $(Al_{0.14}Ga_{0.86})_2O_3$ to AZO and ITO core delta regions. The intensity is in arbitrary units (a.u.).

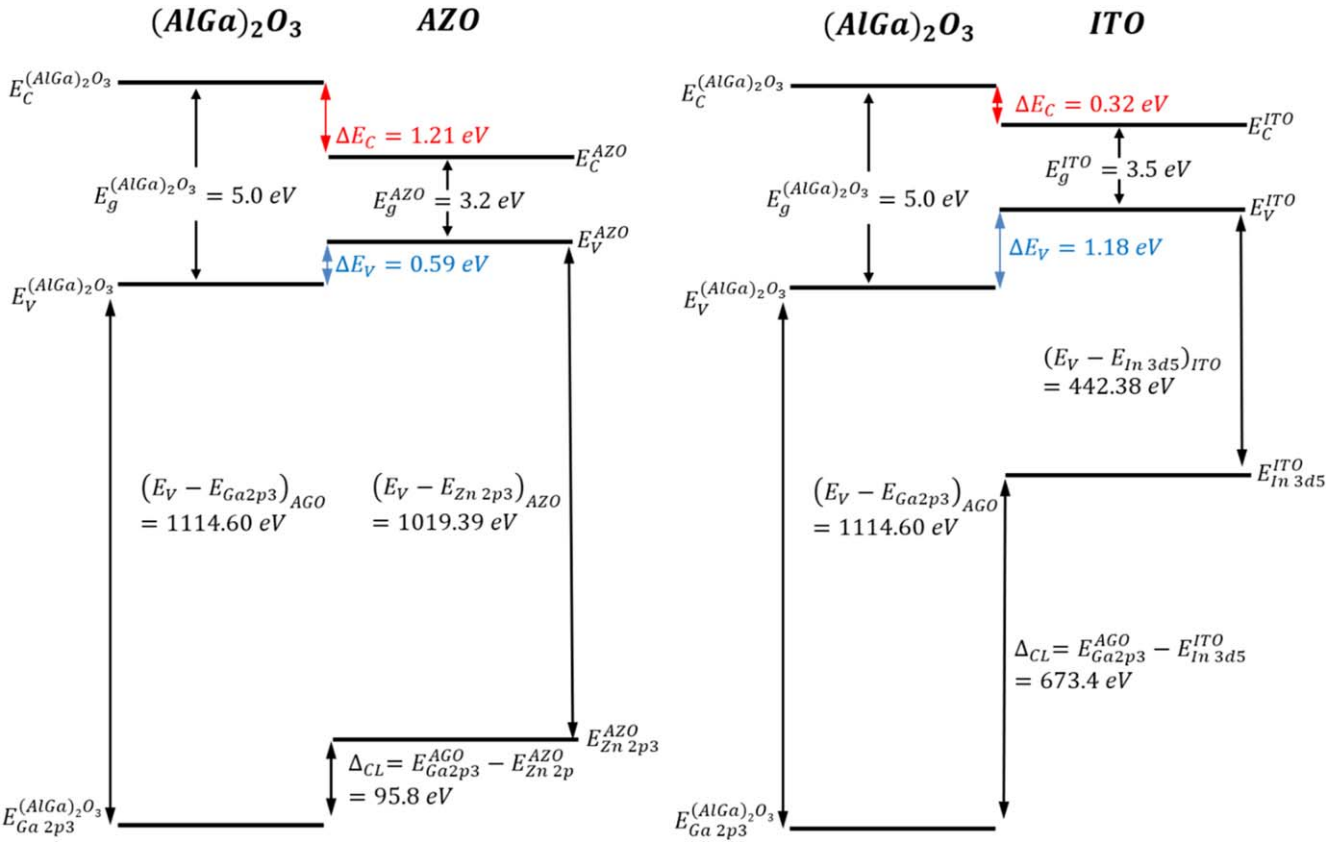

Figure 7. Band diagrams for the AZO (left) and ITO (right) sputtered onto $(Al_{0.14}Ga_{0.86})_2O_3$. The valence band offset was determined to be -0.59 ± 0.08 eV for sputtered AZO and -1.18 ± 0.04 eV for sputtered ITO on β-$(Al_{0.14}Ga_{0.86})_2O_3$. The conduction band offset was 1.21 ± 0.08 eV for AZO and 0.32 ± 0.04 eV for ITO on β-$(Al_{0.14}Ga_{0.86})_2O_3$.

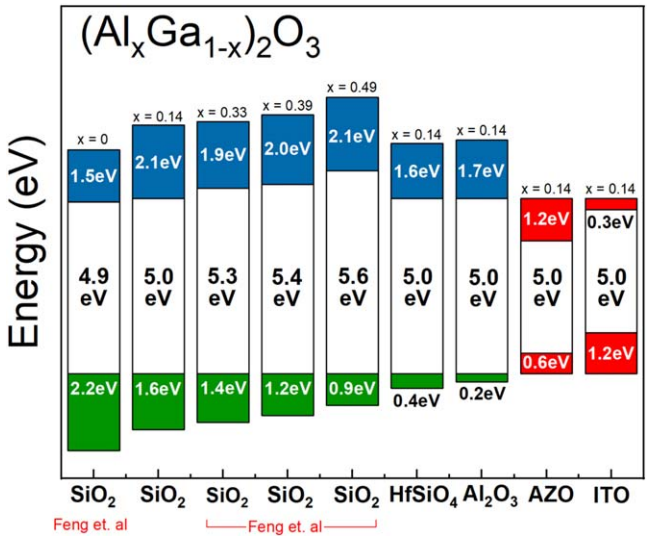

Figure 8. Reported band offsets for various dielectrics on $(Al_xGa_{1-x})_2O_3$ (data from 30] and our work [52, 53]).

differences in bandgaps and the directly measured valence band offset, i.e.: $\Delta E_C = E_g^{\text{AZO or ITO}} - E_g^{\text{AlGaO}} - \Delta E_V$. The band offsets are negative for both oxides on β-$(Al_{0.14}Ga_{0.86})_2O_3$, ensuring good electron and hole transport and hence the ability to reduce contact resistance when used as an interlayer in metal stacks on this wide bandgap material.

To place the work in context, figure 8 shows the reported values for band offsets of dielectrics on $(Al_xGa_{1-x})_2O_3$. All of the reported values to date have been for oxides intended as gate dielectrics [30, 52, 53], which require a larger bandgap than the $(Al_xGa_{1-x})_2O_3$ and typical need conduction band offsets of at least 1 eV to obtain good electron confinement. The work reported in this paper for AZO and ITO shows the negative offsets required for enhancing carrier transport across the heterointerface when used as an interlayer between the metal contact and the $(Al_xGa_{1-x})_2O_3$.

Summary and conclusions

The band alignment at both AZO/β-$(Al_{0.14}Ga_{0.86})_2O_3$ and ITO/β-$(Al_{0.14}Ga_{0.86})_2O_3$ heterojunctions is a nested gap (type I) band offset. The valence and conduction band offsets are negative in both cases, and can be used to enhance carrier transport across the heterointerface. The use of the AZO and ITO interlayers may be a convenient approach for improving Ohmic contact resistance on n-type β-$(Al_xGa_{1-x})_2O_3$.

Acknowledgments

The project or effort depicted was partially sponsored by the Department of the Defense, Defense Threat Reduction Agency, HDTRA1-17-1-011, monitored by Jacob Calkins. The content of the information does not necessarily reflect the position or the policy of the federal government, and no official endorsement should be inferred.

ORCID iDs

S J Pearton https://orcid.org/0000-0001-6498-1256

References

[1] Tadjer M J, Mahadik N A, Freitas J A, Glaser E R, Koehler A D, Luna L E, Feigelson B N, Hobart K D, Kub F J and Kuramata A 2018 Ga_2O_3 Schottky barrier and heterojunction diodes for power electronics applications *Proc. SPIE* **10532** 1053212

[2] Okur S *et al* 2017 Growth of Ga_2O_3 for power device applications *Vac. Technol. Coat.* **5** 31–9

[3] Pearton S J, Yang J, Cary P H IV, Ren F, Kim J, Tadjer M J and Mastro M A 2018 A review of Ga_2O_3 materials, processing, and devices *Appl. Phys. Rev.* **5** 011301

[4] Higashiwaki M and Jessen G H 2018 Guest editorial: the dawn of gallium oxide microelectronics *Appl. Phys. Lett.* **112** 060401

[5] Higashiwaki M, Sasaki K, Murakami H, Kumagai Y, Koukitu A, Kuramata A, Masui T and Yamakosh S 2016 Recent progress in Ga_2O_3 power devices *Semicond. Sci. Technol.* **31** 034001

[6] McGlone J F, Xia Z, Zhang Y, Joishi C, Lodha S, Rajan S, Ringel S A and Arehart A R 2018 Trapping effects in Si δ-doped β-Ga_2O_3 MESFETs on an Fe-doped β-Ga_2O_3 substrate *IEEE Electron Dev. Lett* **39** 1042–5

[7] Tadjer M J, Mahadik N A, Wheeler V D, Glaser E R, Ruppalt L, Koehler A D, Hobart K D, Eddy C R Jr and Kub F J 2016 A (001) β-Ga_2O_3 MOSFET with +2.9 V threshold voltage and HfO_2 gate dielectric *ECS J. Solid State Sci. Technol.* **5** 68–470

[8] Chabak K D *et al* 2018 Recessed-gate enhancement-mode β -Ga_2O_3 MOSFETs *IEEE Electron Dev. Lett.* **39** 67–70

[9] Konishi K, Goto K, Murakami H, Kumagai Y, Kuramata A, Yamakoshi S and Higashiwaki M 2017 1-kV vertical Ga_2O_3 field-plated Schottky barrier diodes *Appl. Phys. Lett.* **110** 103506

[10] Kim J, Oh S, Mastro M and Kim J 2016 Exfoliated β-Ga_2O_3 nano-belt field-effect transistors for air-stable high power and high temperature electronics *Phys. Chem. Chem. Phys.* **18** 15760–4

[11] Singh Pratiyush A, Krishnamoorthy S, Solanke S V, Xia Z, Muralidharan R, Rajan S and Nath D N 2017 High responsivity in molecular beam epitaxy grown β-Ga_2O_3 metal semiconductor metal solar blind deep-UV photodetector *Appl. Phys. Lett.* **110** 221107

[12] Kyrtsos A, Matsubara M and Bellotti E 2018 On the feasibility of p-type Ga_2O_3 *Appl. Phys. Lett.* **112** 032108

[13] Chikoidze E *et al* 2017 P-type β-gallium oxide: a new perspective for power and optoelectronic devices *Mat. Today Phys.* **3** 118–26

[14] Zhang Y *et al* 2018 Demonstration of high mobility and quantum transport in modulation-doped β-$(Al_xGa_{1-x})_2O_3/Ga_2O_3$ heterostructures *Appl. Phys. Lett.* **112** 173502

[15] Krishnamoorthy S, Xia Z, Joishi C, Zhang Y, McGlone J, Johnson J, Brenner M, Arehart A R, Hwang J and Lodha S 2017 Modulation-doped β-$(Al_{0.2}Ga_{0.8})_2O_3/Ga_2O_3$ field-effect transistor *Appl. Phys. Lett.* **111** 023502

[16] Oshima T, Okuno T, Arai N, Kobayashi Y and Fujita S 2009 β-$Al_{2x}Ga_{2-2x}O_3$ thin film growth by molecular beam epitaxy *Japan. J. Appl. Phys.* **8** 070202

[17] Oshima T, Kato Y, Kawano N, Kuramata A, Yamakoshi S, Fujita S, Oishi T and Kasu M 2017 Carrier confinement observed at modulation-doped β-$(Al_xGa_{1-x})_2O_3/Ga_2O_3$ heterojunction interface *Appl. Phys. Express* **10** 035701

[18] Oshima Y, Ahmadi E, Badescu S C, Wu F and Speck J S 2016 Composition determination of β-$(Al_xGa_{1-x})_2O_3$ layers coherently grown on (010) β-Ga_2O_3 substrates by high-resolution x-ray diffraction *Appl. Phys. Express* **9** 061102

[19] Kaun S W, Wu F and Speck J S 2015 β-$(Al_xGa_{1-x})_2O_3/Ga_2O_3$ (010) heterostructures grown on β-Ga_2O_3 (010) substrates by plasma-assisted molecular beam epitaxy *J. Vac. Sci. Technol.* A **33** 041508

[20] Zhang Y, Joishi C, Xia Z, Brenner M, Lodha S and Rajan S 2018 Demonstration of β-$(Al_xGa_{1-x})_2O_3/Ga_2O_3$ double heterostructure field effect transistors *Appl. Phys. Lett.* **112** 233503

[21] Zhang F, Saito K, Tanaka T, Nishio M, Arita M and Guo Q 2014 Wide bandgap engineering of $(AlGa)_2O_3$ films *Appl. Phys. Lett.* **105** 162107

[22] Oshima T *et al* 2016 Formation of indium-tin oxide ohmic contacts for β-Ga_2O_3 *Japan. J. Appl. Phys.* **55** 1202B7

[23] Yao Y, Davis R F and Porter L M 2016 Investigation of different metals as ohmic contacts to β-Ga_2O_3: comparison and analysis of electrical behavior, morphology, and other physical properties *J. Electron. Mater.* **46** 2053–960

[24] Carey P H IV, Ren F, Hays D C, Gila B P, Pearton S J, Jang S and Kuramata A 2017 Valence and conduction bandoffsets in AZO/Ga_2O_3 heterostructures *Vacuum* **141** 103–8

[25] Carey P H, Yang J, Ren F, Hays D C, Pearton S J, Jang S, Kuramata A and Kravchenko I I 2017 Ohmic contacts on N-type Ga_2O_3 using AZO/Ti/Au *AIP Adv.* **7** 095313

[26] Carey P H, Ren F, Hays D C, Gila B P, Pearton S J, Jang S and Kuramata A 2017 Band offsets in ITO/Ga_2O_3 heterostructures *Appl. Surf. Sci.* **422** 179–83

[27] Carey P H IV, Yang J, Ren F, Hays D C, Pearton S J, Kuramata A and Kravchenko I I 2017 Improvement of ohmic contacts on Ga_2O_3 through use of ITO-interlayers *J. Vac. Sci. Technol.* B **35** 061201

[28] Wakabayashi R, Hattori M, Yoshimatsu K, Horiba K, Kumigashira H and Ohtomo A 2018 Band alignment at β-$(Al_xGa_{1-x})_2O_3/\beta$-$Ga_2O_3$ (100) interface fabricated by pulsed-laser deposition *Appl. Phys. Lett.* **112** 232103

[29] Peelaers H, Varley J B, Speck J S and Van de Walle C G 2018 Structural and electronic properties of Ga_2O_3–Al_2O_3 alloys *Appl. Phys. Lett.* **112** 242101

[30] Feng Z, Feng Q, Zhang J, Li X, Li F, Huang L, Chen H-Y, Lu H-L and Hao Y 2018 Band alignment of $SiO_2/(Al_xGa_{1-x})_2O_3$ ($0 \geqslant x \leqslant 0.49$) determined by x-ray photoelectron spectroscopy *Appl. Surf. Sci.* **434** 440–44

[31] Jia Y, Zheng K, Wallace J S, Gardella J A and Singisetti U 2015 Spectroscopic and electrical calculation of band alignment between atomic layer deposited SiO_2 and β-Ga_2O_3 ($2^{-}01$) *Appl. Phys. Lett.* **106** 102107

[32] Konishi K, Kamimura T, Wong M H, Sasaki K, Kuramata A, Yamakoshi S and Higashiwaki M 2016 Large conduction band offset at SiO_2/β-Ga_2O_3 heterojunction determined by x-ray photoelectron spectroscopy *Phys. Status Solidi* b **253** 623–5

[33] Kamimura T, Sasaki K, Wong M H, Krishnamurthy D, Kuramata A, Masui T, Yamakoshi S and Higashiwaki M 2014 Band alignment and electrical properties of Al_2O_3/β-Ga_2O_3 heterojunctions *Appl. Phys. Lett.* **104** 192104

[34] Wheeler V D, Shahin D I, Tadjer M J and Eddy C R Jr 2017 Band alignments of atomic layer deposited ZrO_2 and HfO_2 high-k dielectrics with (−201) β-Ga_2O_3 *ECS J. Solid State Sci. Technol.* **6** Q3052–5

[35] Carey P H, Ren F, Hays D C, Gila B P, Pearton S J, Jang S and Kuramata A 2017 Conduction and valence band offsets of $LaAl_2O_3$ with (−201) β-Ga_2O_3 *J. Vac. Sci. Technol.* B **35** 041201

[36] Carey P, Ren F, Hays D C, Gila B P, Pearton S J, Jang S and Kuramata A 2017 Band alignment of atomic layer deposited SiO_2 and $HfSiO_4$ with β-Ga_2O_3 *Japan. J. Appl. Phys.* **56** 071101

[37] Carey P, Ren F, Hays D C, Gila B P, Pearton S J, Jang S and Kuramata A 2017 Band alignment of Al_2O_3 with (−201) β-Ga_2O_3 *Vacuum* **142** 52–7

[38] Hays D C, Gila B P, Pearton S J, Trucco A, Thorpe R and Ren F 2017 Effect of deposition conditions and composition on band offsets in atomic layer deposited $Hf_xSi_{1-x}O_y$ on $InGaZnO_4$ *J. Vac. Sci. Technol.* B **35** 011206

[39] Hays D C, Gila B P, Pearton S J and Ren F 2017 Energy band offsets of dielectrics on $InGaZnO_4$ *Appl. Phys. Rev.* **4** 021301

[40] Kraut E A, Grant R W, Waldrop J R and Kowalczyk S P 1980 Precise determination of the valence-band edge in x-ray photoemission spectra: application to measurement of semiconductor interface potentials *Phys. Rev. Lett.* **44** 1620–4

[41] Jeong S H and Boo J H 2004 Influence of target-to-substrate distance on the properties of AZO films grown by rf magnetron spuittering *Thin Solid Films* **447/448** 105–10

[42] Bender M, Seelig W, Daube C, Frankenberger H, Ocker B and Stollenwerk J 1998 Dependence of oxygen flow on optical and electrical properties of DC-magnetron sputtered ITO films *Thin Solid Films* **326** 72–7

[43] Wu W F, Chiou B S and Hsieh S T 1994 Effect of sputtering power on the structural and optical properties of rf magnetron sputtered ITO films *Semicond. Sci. Technol.* **9** 1242–9

[44] Kuramata A 2018 private communication

[45] Bersch E, Di M, Consiglio S, Clark R D, Leusink G J and Diebold A C 2010 Complete band offset characterization of the $HfO_2/SiO_2/Si$ stack using charge corrected x-ray photoelectron spectroscopy *J. Appl. Phys.* **107** 043702

[46] Shin H C, Tahir D, Seo S, Denny Y R, Oh S K, Kang H J, Heo S, Chung J G, Lee J C and Tougaard S 2012 Reflection electron energy loss spectroscopy for ultrathin gate oxide materials *Surf. Interface Anal.* **44** 623

[47] Klein A 2015 Energy band alignment in chalcogenide thin film solar cells from photoelectron spectroscopy *J. Phys.: Condens. Matter* **27** 134201

[48] Chen F, Schafranek R, Li S, Wu W and Klein A J 2010 Energy band alignment between Pb(Zr, Ti)O_3 and high and low work function conducting oxides—from hole to electron injection *J. Phys. D: Appl. Phys.* **43** 295301

[49] Li S *et al* 2014 Intrinsic energy band alignment of functional oxides *Phys Status Solidi* **8** 571–6

[50] Guo X, Zheng H, King S W, Afanas'ev V V, Baklanov M R, Marneffe J-F D, Nishi Y and Shohet J L 2015 Defect-induced bandgap narrowing in low-k dielectrics *Appl. Phys. Lett.* **107** 082903

[51] Krueger B W, Dandeneau C S, Nelson E M, Dunham S T, Ohuchi F S and Olmstead M A 2016 Variation of band gap and lattice parameters of β-$(Al_xGa_{1-x})_2O_3$ powder produced by solution combustion synthesis *J. Am. Ceram. Soc.* **99** 2467–73

[52] Fares C, Ren F, Lambers E, Hays D C, Gila B P and Pearton S J 2018 Band alignment of atomic layer deposited SiO_2 on (010) $(Al_{0.14}Ga_{0.86})_2O_3$ *J. Vac. Sci. Technol.* B **36** 061207

[53] Fares C, Ren F, Lambers E, Hays D C, Gila B P and Pearton S J 2018 Band offsets for atomic layer deposited $HfSiO_4$ on $(Al_{0.14}Ga_{0.86})_2O_3$ *ECS J. Solid State Sci. Technol.* **7** P519–23